

Derivation of the MODIS Aqua Point-Spread Function for Ocean Color Bands

Gerhard Meister^a, Yuqin Zong^b, and Charles R. McClain^c

^aFuturetech Corp., NASA Ocean Biology Processing Group, Code 614.2, Goddard Space Flight Center, Greenbelt, MD 20771, USA;

^bNational Institute of Standards and Technology, Gaithersburg, MD 20899, USA;

^cNASA, Ocean Biology Processing Group, Code 614.2, Goddard Space Flight Center, Greenbelt, MD 20771, USA

ABSTRACT

The Moderate Resolution Imaging Spectroradiometer (MODIS) on the Earth Observing System (EOS) Aqua platform has 9 spectral bands with center wavelengths from 412nm to 870nm that are used to produce the standard ocean color data products. Ocean scenes usually contain high contrast due to the presence of bright clouds over dark water. The MODIS has been characterized for straylight effects prelaunch. In this paper, we derive Point-Spread Functions for the MODIS Aqua ocean bands based on the prelaunch Near-Field Response measurements. We use Harvey-Shack coefficients derived by the system vendor Santa Barbara Remote Sensing. The crucial step in the derivation of the Point-Spread Function is the normalization of the Harvey-Shack coefficients relative to the center pixel. The straylight contamination of ocean scenes is evaluated based on artificial test scenes. Furthermore, the dependence of top-of-atmosphere radiances and ocean color products on proximity to a cloud is analyzed, and a straylight correction algorithm is proposed.

Keywords: MODIS, point-spread function, scanner, characterization

1. INTRODUCTION

This paper presents an estimate of the stray light effects in the MODIS (Moderate Resolution Imaging Spectroradiometer, see Barnes et al.¹ on NASA's EOS (Earth Observing Systems) Aqua satellite. The focus of this investigation is on the MODIS ocean color bands (MODIS bands 8-16, corresponding to wavelengths from 412nm to 870nm), which all have a nadir resolution of 1km x 1km. MODIS is a scanning radiometer, with 10 detectors simultaneously recording for the ocean color bands, resulting in a scan line of 10 x 1354 pixels.

A Point-Spread Function (PSF) is required to correct for straylight artifacts that are associated with contamination of the currently viewed pixel by light from outside the nominal FOV (field-of-view) of the current pixel. The PSF is defined here as

$$L_m(x_0, y_0) = \sum_{i,j} PSF(i - x_0, j - y_0) \cdot L_T(i, j) \quad (1)$$

where $L_m(x_0, y_0)$ is the measured radiance from pixel (x_0, y_0) , L_T is the true radiance. The summation is supposed to cover all directions from which light enters the sensor, but is in practice limited by the actual size of the image. The PSF is normalized to 1:

$$\sum_{i,j} PSF(i, j) = 1 \quad (2)$$

The first part of this paper (sections 2 and 3) describes the PSF model creation. The second part (section 4) applies the PSF to artificial scenes, showing that even at a distance of 50 pixels from a large cloud, the correction can be significant. The intensity of the correction depends strongly on the size of the cloud and varies from band to band. The 5th section looks at cloud edge effects in real images, the sixth section discusses a possible correction algorithm.

Further author information:

G.M.: E-mail: Gerhard.Meister@nasa.gov

2. PRELAUNCH CHARACTERIZATION

MODIS was characterized by Santa Barbara Remote Sensing (SBRS), California. Line-Spread Functions (LSFs) were acquired along-scan and along-track in two different modes:

1. varying the slit position by fractions of a pixel to determine the Modulation Transfer Function (MTF), and
2. keeping the slit position constant, but inserting neutral density filters and measuring at different light intensities.

With the second method, the response of pixels far away from the slit measured with a high light intensity (so high that the slit measurements actually saturate) can be related to measurements of low light intensity where the slit does not saturate. This type of LSF is called Near-Field Response (NFR) by SBRS, see Hurt and Derrick.² The dynamic range of the MTF measurements is about 10^3 , for the NFR measurements it is about 10^7 . In order to characterize the system response to a bright target located several pixels away, NFR measurements are needed. MODIS NFR was only characterized in the along-scan direction, not in the along-track direction. MODIS MTF was characterized for both directions.

The MODIS Aqua NFR measurements are described by Harvey-Shack functions by Derrick.³ The model was created for MODIS by Young.⁴ It predicts the measured response for pixels further than 1 pixel away from the slit. The model either uses one or a combination of two Harvey-Shack functions, depending on whether the light was scattered outside or inside of the MODIS field baffle. The NFR measurements are only available for detector 5.

3. DERIVATION OF THE PSF

The general shape of the PSF is given by the Harvey-Shack based model from SBRS. The along-track scattering Harvey-Shack parameters are assumed to be identical to the along-scan parameters. The crucial issue for the creation of the PSF is the normalization of the SBRS model relative to the center pixel. The approach chosen here is to estimate the PSF of the central 3x3 pixels based on

- the LSFs in the along-track direction measured for the MTF characterization (see e.g. Barnes et al.,¹ Fig. 3a), and
- the theoretical value for the adjacent pixel in scan direction from Nishihama et al.⁵

The results are given in Table 1 as a function of $p_0 = PSF(0,0)$, the value of the PSF for the central pixel (x_0, y_0), i.e. the maximum of the PSF.

Table 1. Modeled PSF of the central 3 pixels.

Scan Index	Track Index	Value
0	0	p_0
± 1	0	$0.125/0.75 \cdot p_0$
0	± 1	$0.05 \cdot p_0$
± 1	± 1	$0.125/0.75 \cdot 0.05 \cdot p_0$

The normalization constant for the Harvey-Shack model and p_0 are then optimized so that the resulting PSF reproduces the NFR measurements. The sum of the PSF of the central 3x3 pixels for MODIS Aqua band 11 is 0.9971. For MODIS Terra, Qiu et al.⁶ reported a value of 0.9932 for band 11, i.e. significantly more scatter than we find in MODIS Aqua. The agreement between modeled and measured NFR is shown in Fig.1 for Aqua band 11, the modeled PSF is shown in Fig.1 as well. All 10 detectors are assumed to have the same Harvey-Shack coefficients as detector 5, but their PSFs are different due to their different position on the focal plane relative

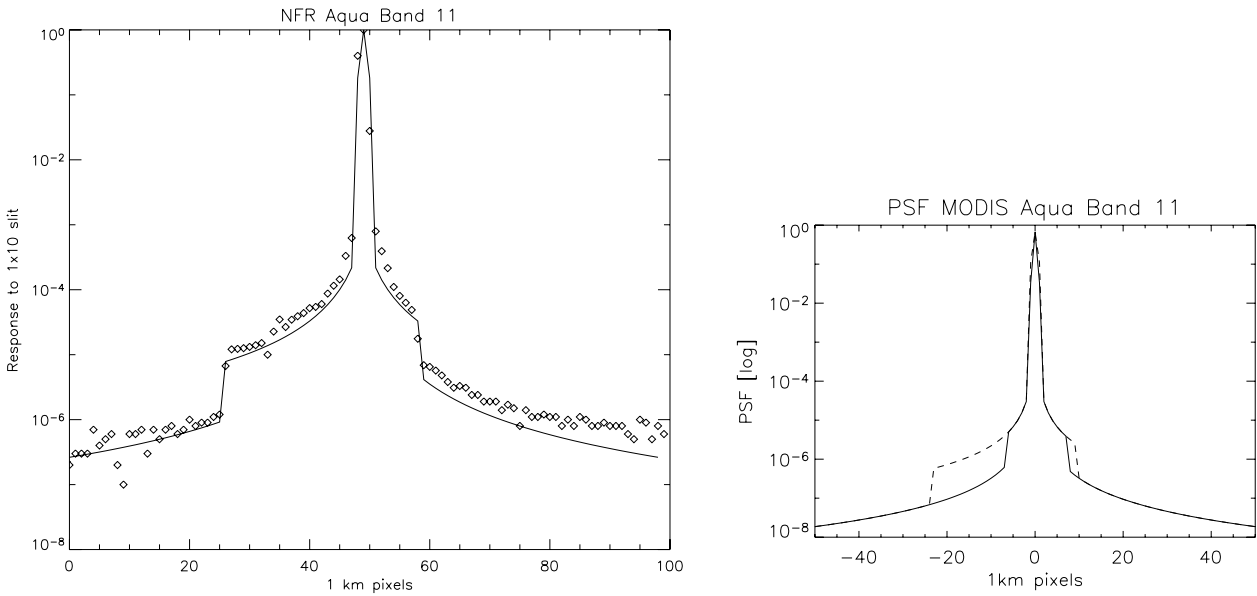


Figure 1. Left: NFR measurements (diamonds) and NFR modeled from PSF (solid line) for MODIS Aqua band 11. Right: MODIS Aqua band 11 PSF in track direction (solid line) and scan direction (dashed line).

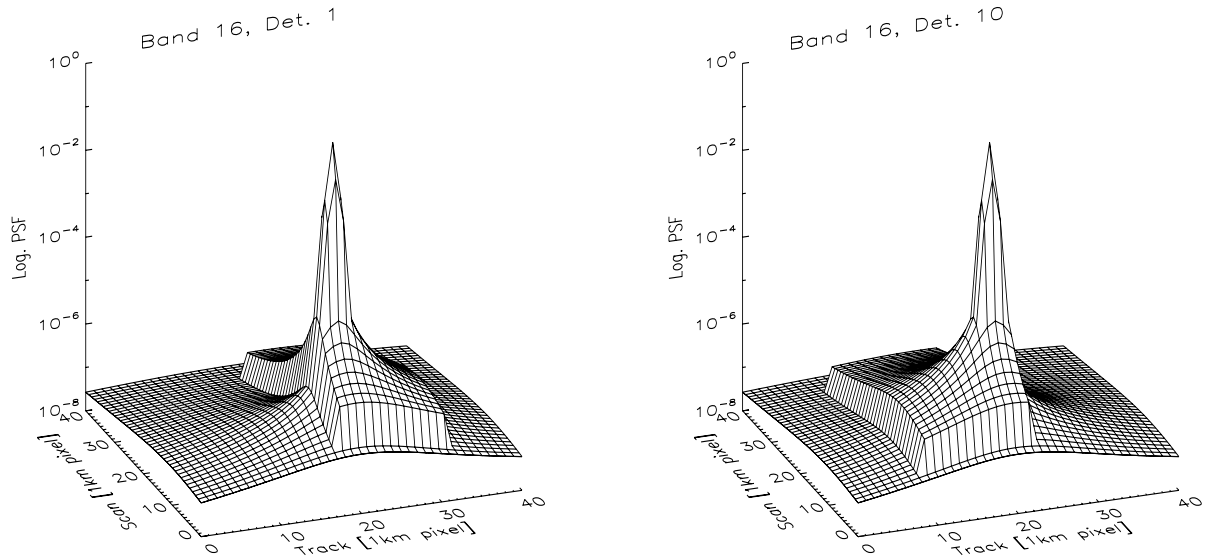


Figure 2. Modeled MODIS Aqua PSF for band 16, detector 1 (left) and detector 10 (right).

to the MODIS field baffle, which can be seen in Fig. 2. Note also that position of the band on the focal plane influences its PSF: bands 11 and 16 are on different sides of the focal plane, and the PSF plateau in scan direction is longer before the peak in band 11 (Fig.1), but longer after the peak in band 16 (Fig. 2).

The equivalent of the NFR plot in Fig.1 has been shown in Qiu et al.⁶ for MODIS Terra. Qualitatively, the NFR measurements of both MODIS instruments are similar, but the MODIS Aqua NFR measurements are generally lower, i.e. there is more stray light in MODIS Terra.

The measured NFR values in Fig.1 are slightly higher than the modeled values after the peak (right side of Fig.1). Generally, data measured after the peak are less reliable due to hysteresis of the detectors and were not used in the fitting of the Harvey-Shack parameters by Derrick (2002).

The equivalent of the PSF plot in Fig.1 is also shown in Qiu et al.⁶ for MODIS Terra. 30 pixels away from the center peak, the PSF of MODIS Terra is a little less than 1×10^{-6} , whereas for MODIS Aqua it is 4.5×10^{-8} . Unfortunately, the PSF model used in Qiu et al.⁶ is unavailable, the publication is the only source of information we can use.

4. APPLICATION TO TEST IMAGES

Following the method outlined in Qiu et al.,⁶ an artificial image with 512x512 pixel was created with the left (or right) half of the image containing cloud radiances (Lcloud), the other half typical radiances (Ltyp; a ratio Lcloud/Ltyp of exactly 20 was chosen in Fig.3 to ensure comparability to data in Qiu et al.⁶). Qiu did not define if the cloud is at the beginning of the scan (BOS) or end of scan (EOS), so we calculated both cases. The PSF was applied to the artificial image to simulate the scattering of MODIS Aqua. The radiance error is the difference of the simulated image with scatter and the artificial input image. The results are shown in Fig.3 as a function of the distance to the cloud. The values for MODIS Terra were read from the figure in Qiu et al.,⁶ and are therefore only approximate. It can be seen that the contamination of MODIS Aqua band 11 top-of-atmosphere radiances due to a large cloud is significant (1% contamination 8km or 13km away from the cloud, for the cloud being at the beginning or end of scan, respectively), but the contamination is much less than for MODIS Terra (1% contamination 21 pixels away from the cloud).

Fig. 4 shows the expected response at the edge of a semi-infinite cloud for all MODIS Aqua bands, using a ratio Lcloud/Ltypical of 20 for all bands. Although this is not realistic, it shows the spectral dependence of the sensor inherent straylight effects due to the PSF very well. Bands 8-10 have the highest straylight effects for a constant ratio Lcloud/Ltypical, bands 11-16 are all very similar.

A more realistic estimation of the straylight effects in ocean scenes uses the ratio Lcloud/Ltypical given in table 2, the results are shown in Fig. 5. Band 11 happens to be the band with the lowest straylight effects, band 13 has by far the highest. Bands 15 and 16 have very similar straylight effects, which is an advantage for the ocean color atmospheric correction. Note that band 13 has a much stronger straylight response than band 14. This could be a problem for the fluorescence line height (FLH) algorithm, which critically depends on the radiance difference between those two bands. But it is not clear whether the stray light response difference between bands 13 and 14 is real or a characterization artifact, because there is no reason the stray light characteristic should be that different for two bands whose wavelengths are so close together, see table 2.

The cloud used in Fig.3 is very large. The effect from a much smaller cloud (only 10x10 pixels) can be seen in Fig.6, using ratios Lcloud/Ltyp from table 2, e.g., 10 pixels away from the cloud, the contamination is 0.225% for band 11.

The strong variation of straylight contamination among the bands is partly due to the different Lcloud/Ltyp ratios, and partly due to different PSFs (see the strong variation in the sum of the PSF of the central 3x3 pixels shown in table 2. The between band variation is problematic for the ocean color products, because often stray light is removed from the ocean color products because it is (erroneously) characterized as aerosol contribution; the quality of the derived products suffers if the stray light contribution is wavelength dependent.

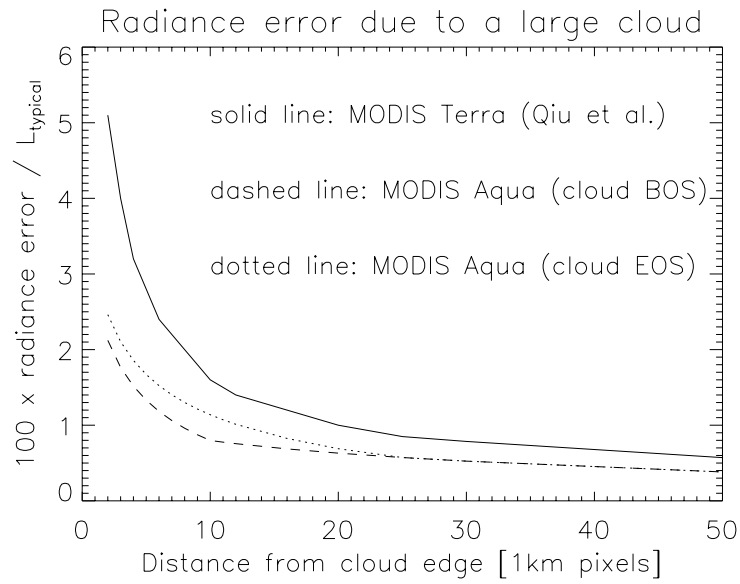


Figure 3. Contamination of top-of-atmosphere radiances over ocean due to a large cloud (semi-infinite) for band 11.

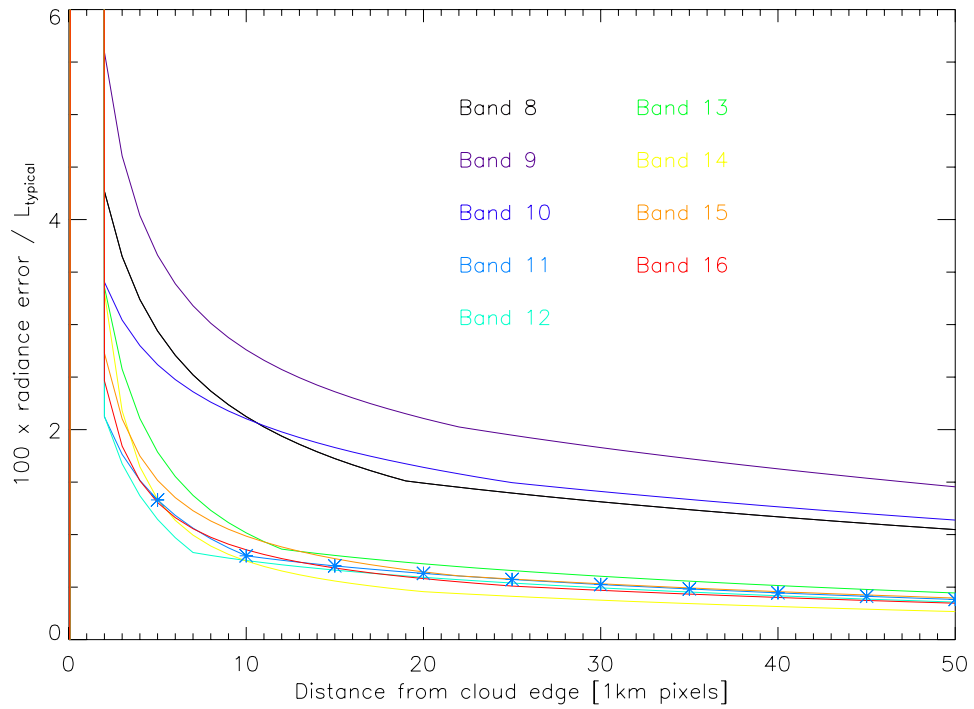


Figure 4. Contamination of top-of-atmosphere radiances over ocean due to a large cloud (semi-infinite) for bands 8-16. The cloud is at the end of the scan (EOS). Stars indicate band 11 for better readability. Ratio $L_{\text{cloud}}/L_{\text{typical}}$ is 20 for all bands.

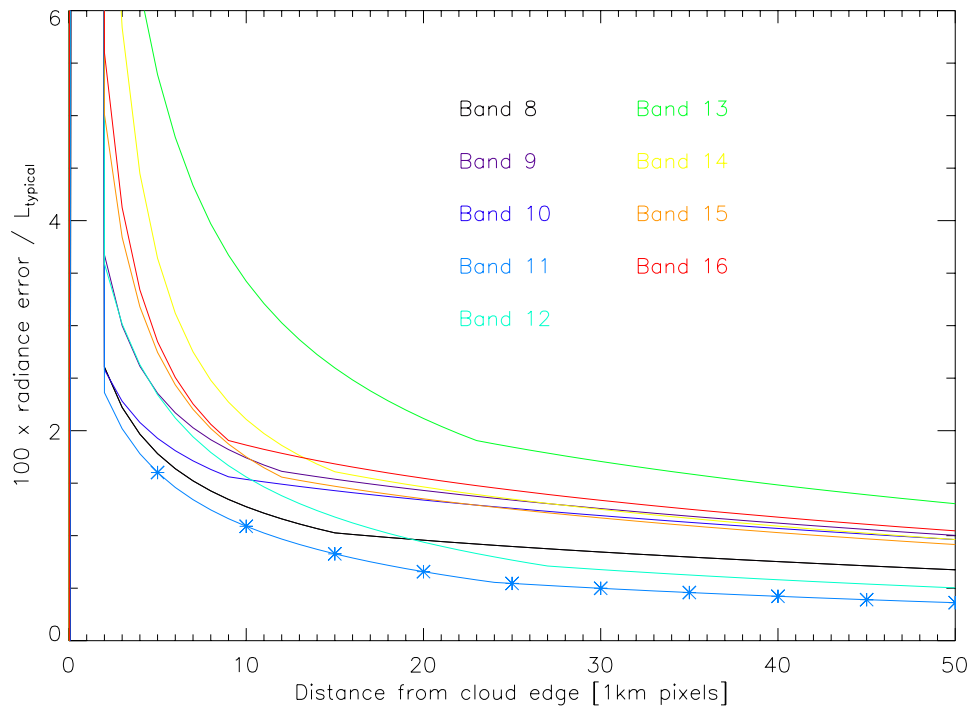


Figure 5. Contamination of top-of-atmosphere radiances over ocean due to a large cloud (semi-infinite) for bands 8-16. The cloud is at the EOS. Stars indicate band 11 for better readability. Ratio $L_{\text{cloud}}/L_{\text{typical}}$ is taken from table 2.

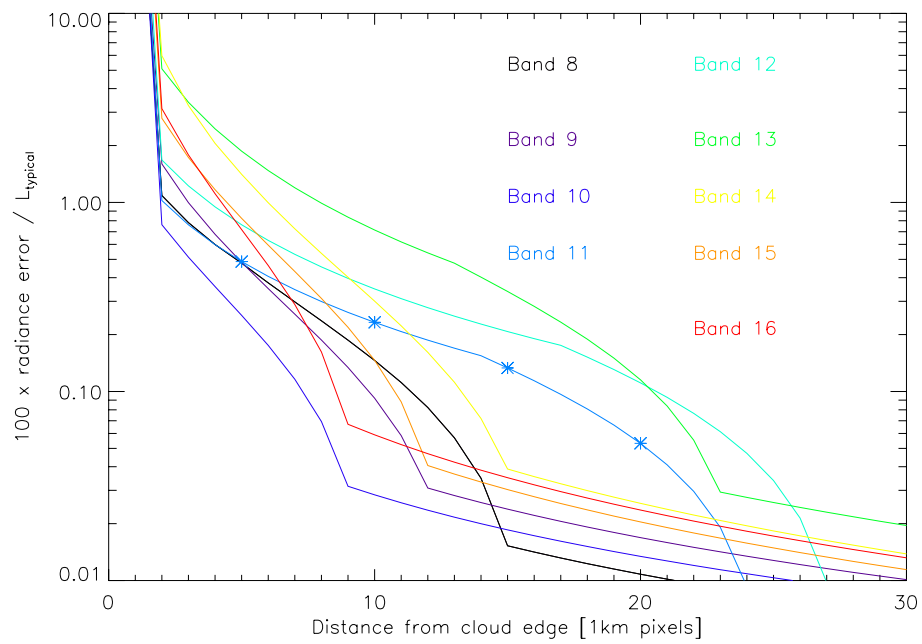


Figure 6. Contamination of top-of-atmosphere radiances over ocean due to a small cloud (10x10 pixels) at the EOS.

Table 2. Specifications for the MODIS ocean color bands and ratio of 3x3 central PSF pixels to total PSF (i.e. PSF with 512x512 elements) for MODIS Aqua. Radiance units are $W/(m^2\mu m sr)$.

Band	8	9	10	11	12	13	14	15	16
Center Wavelength [nm]	412	443	488	531	551	667	678	748	869
Ltypical	44.9	41.9	32.1	27.9	21.0	9.5	8.7	10.2	6.2
Lcloud	573	585	539	538	528	471	440	373	286
Ratio Lcloud/ Ltypical	12.8	14.0	16.8	19.3	25.1	49.6	46.3	36.6	46.1
PSF(3x3)/PSF(512x512)	0.9952	0.9933	0.9965	0.9973	0.9970	0.9956	0.9954	0.9967	0.9970

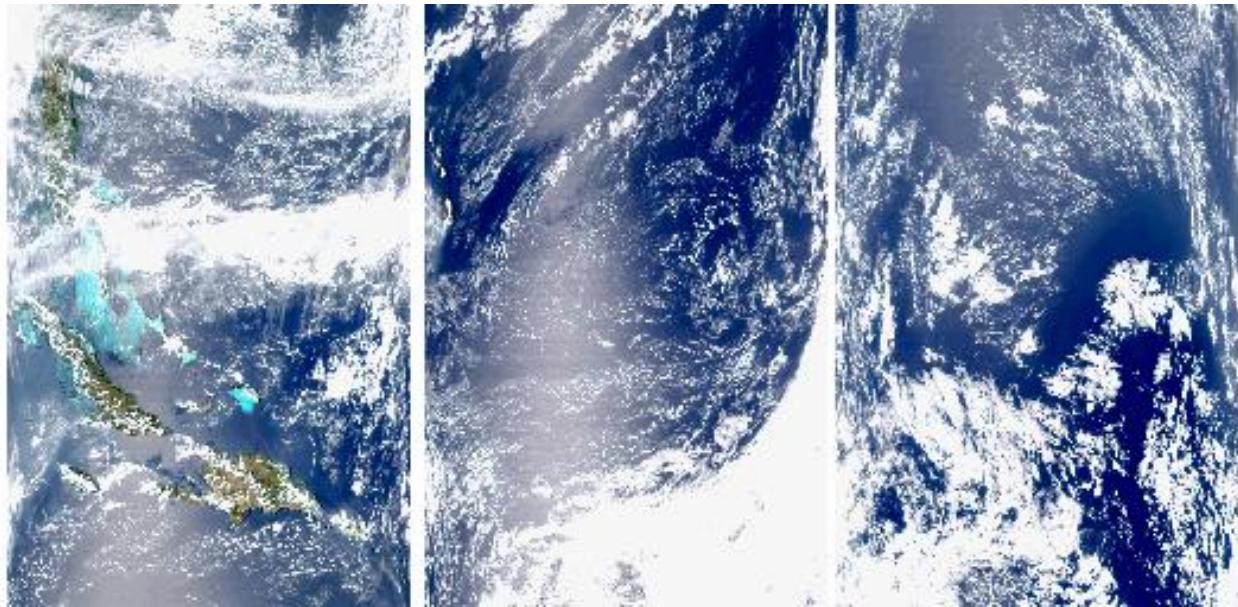


Figure 7. True color image of MODIS Aqua granules A20030701810, A20030702305, and 20031271435 (left to right).

5. CLOUD EDGE EFFECTS IN REAL IMAGES

Straylight effects will appear in ocean images as elevated top-of-atmosphere (TOA) radiances L_t of ocean pixels in the vicinity of clouds. It is important to note that an increase of L_t next to clouds is expected due to scattering effects in the atmosphere or subpixel clouds. To predict the magnitude of this increase is a topic of current scientific investigations.^{7,8}

As an initial step, a simple algorithm was used to quantify the increase of the radiances in the vicinity of clouds. We processed three MODIS granules (see Fig.7) with SeaDAS (provide citation) from L1A to TOA radiances. We then used the SeaDAS cloud flag, and calculated the average radiance of all the ocean pixels adjacent to the cloud flag (either in track or scan direction, or diagonal). These pixels were labeled with 'Distance to cloud 1'. In the case of a 1 cloud pixel, the average was taken over a 3x3 square, without the center pixel. Then we calculated the average of all the pixels adjacent to the pixels labeled 'Distance to cloud 1', and labeled them 'Distance to cloud 2'. If a pixel was already labeled with 'Distance 1', it was not included in the second average. So in case of a 1 cloud pixel, the 'Distance to cloud 2' pixels were a 5x5 square around the cloud, without the central 3x3 square. This was continued until we reached 'Distance to cloud 39'.

The number of pixels for each 'Distance to cloud' is shown in Fig. 8. It can be seen that most of the

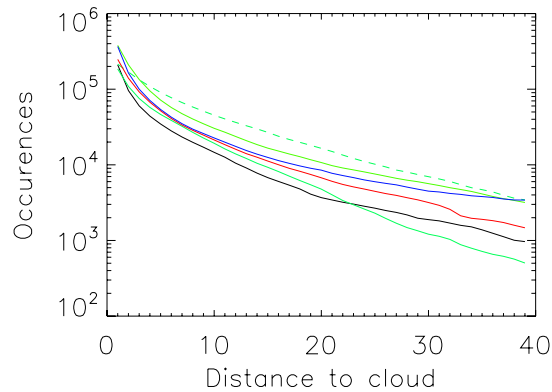


Figure 8. The number of occurrences (or number of pixels) for each 'Distance to cloud' in the investigated data files. The black, red, and blue lines are for Aqua granules A20030701810, A20030702305, and 20031271435, resp. The green lines are for SeaWiFS MLAC data, files S2003070224619 and S1999117171012 (only scan lines 4712 to 7439 were used from the first file, lines 4512 to 7254 from the second file, and lines 10000 to 12900 from the second file (dashed line)).

ocean pixels are actually very close to clouds (note the logarithmic scale). About half of the ocean pixels are within a 5x7 mask around clouds (a 5x7 mask is used in the operational ocean color processing to flag straylight contaminated pixels; these pixels are not used to calculate level 3 data in the operational processing). Excluding those pixels, the average 'Distance to cloud' is still about 12. So the true typical distance between a cloud edge and an nLw retrieval is probably between 15km and 20km (considering that 1) the 'Distance to cloud' as defined here is actually a square and not a circle, and 2) the distance between pixels in scan direction increases for high scan angles).

The average L_t for each set of pixels 'Distance to cloud x ' (with $1 \leq x < 40$) is shown in Fig. 9. It can be seen that the radiances increase significantly when approaching a cloud, by about 5% for the shorter wavelength bands, by up to 40% for the NIR bands. As noted above, this increase is most likely due to both a real increase of the TOA radiances and scattering due to the sensor. Part of the reason for the increase could also be that it is more likely to find a large, cloud-free area at nadir than at the edge of the scan (L_t is lower at nadir than at the edge of the scan by about 50%). It is not clear why the radiances are often lower at 'Distance of cloud 20' versus 'Distance to cloud 39', it is possible that the small number of pixels at large distances does not yield a representative sampling. Note that the MODIS Aqua cloud mask (covering two/three pixels adjacent to a cloud in track/scan direction) excludes the steepest part of the curves from ocean color processing.

Fig. 9 also shows the results for SeaWiFS⁹ data (MLAC data files S2003070224619 and S1999117171012). SeaWiFS has more sensor intrinsic straylight than MODIS Aqua, but a straylight correction has been applied to the SeaWiFS data.¹⁰ It can be seen that the results are qualitatively similar to MODIS Aqua, which suggests that indeed the features we see are mainly due to scattering processes in the atmosphere. Based on the very limited amount of data used in this study, it seems that the rise of L_t when approaching a cloud is steeper in Aqua than in SeaWiFS.

Fig. 10 shows several ocean color products as a function of 'Distance to cloud'. It can be seen that there is a general trend of the water-leaving radiances to increase when approaching a cloud. The aerosol optical thickness (AOT) shows a drastic increase when approaching a cloud, epsilon (a quantity used to determine the aerosol type, see Gordon and Wang¹¹) does not show a consistent behavior. The analysis of these results is still in progress. The variation between the curves in the chlorophyll plot suggests that many more granules are needed to derive an average trend. However, it is encouraging that the two MODIS curves for granules with deep water only (blue and red) are generally similar (the black line is for the MODIS granule containing coastal regions and its pattern is clearly different from the blue and red line, especially for chlorophyll).

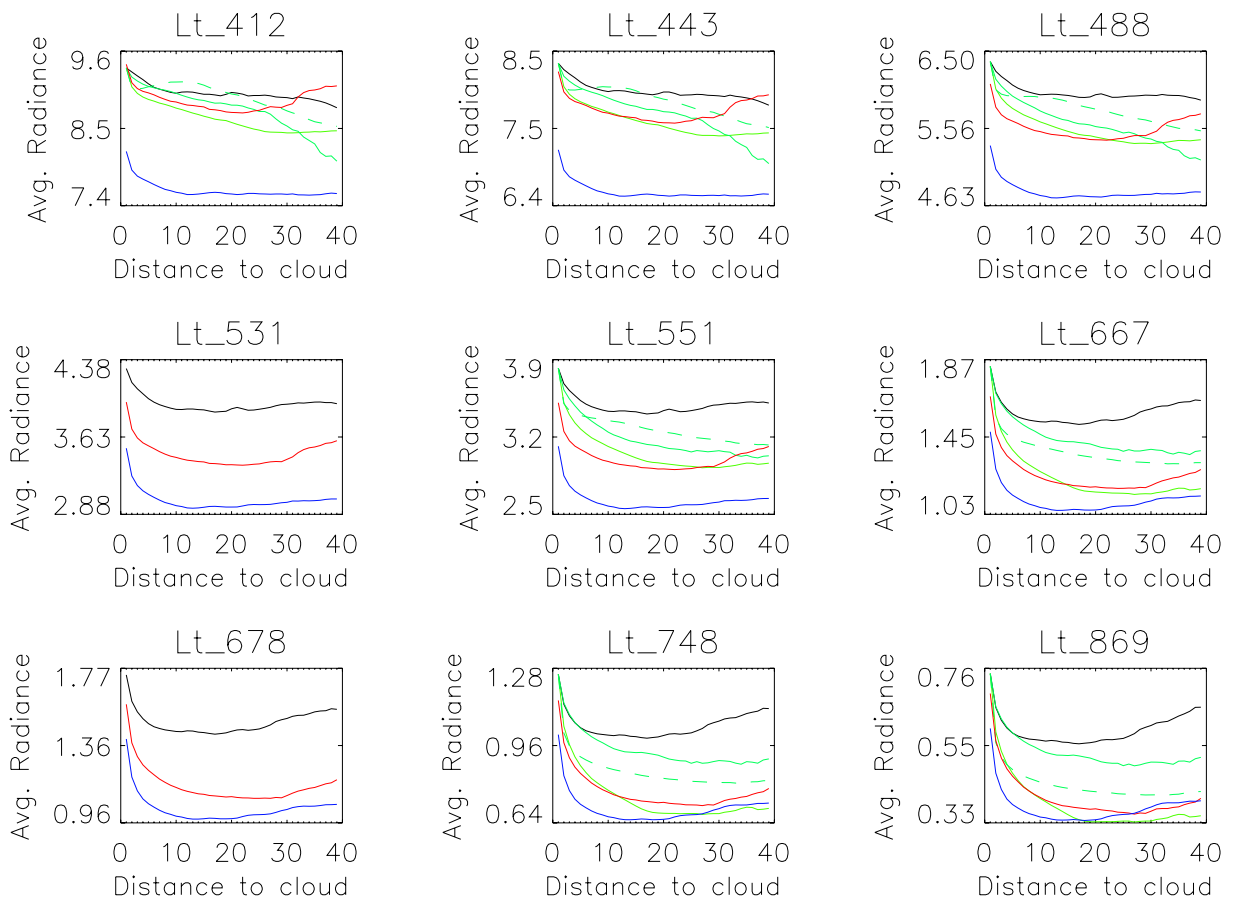


Figure 9. The average radiances for each set of pixels 'Distance to cloud x ' (with $1 \leq x < 40$) for MODIS Aqua bands 8-16. Radiance unit is $mW/(cm^2 sr \mu m)$. The black, red, and blue lines are for granules A20030701810, A20030702305, and 20031271435, resp. The green lines are for SeaWiFS MLAC data, see caption of Fig. 8. To fit the plotting range, SeaWiFS radiances (bands 1-3 and 5-8) were normalized to the starting point of the black line. MODIS bands 11 and 14 (531nm and 678nm) have no direct equivalent in SeaWiFS.

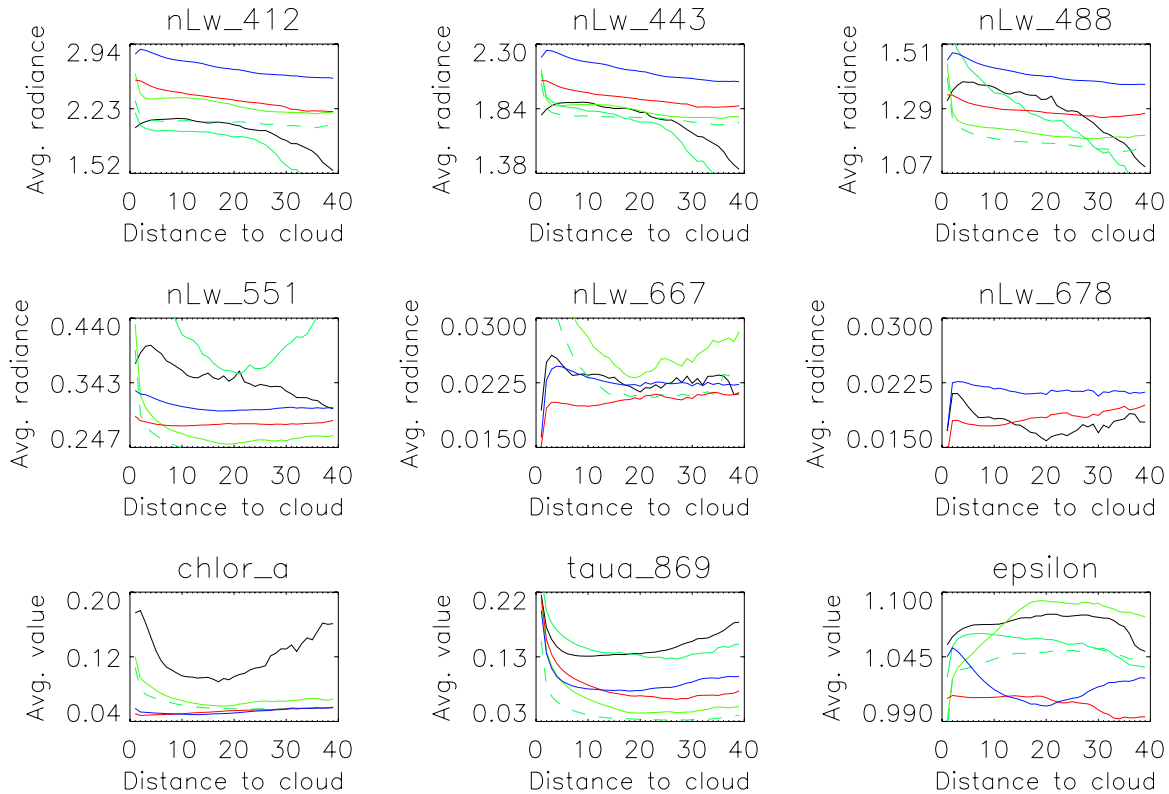


Figure 10. Average ocean color products for each set of pixels 'Distance to cloud x ' (with $1 \leq x < 40$) for MODIS Aqua and SeaWiFS. Water-leaving radiance (nLw) unit is $mW/(cm^2 sr \mu m)$, chlorophyll unit is mg/m^3 , AOT (taua) and epsilon are dimensionless. The black, red, and blue lines are for granules A20030701810, A20030702305, and 20031271435, resp. The green lines are for SeaWiFS MLAC data, see caption of Fig. 8. The missing SeaWiFS line for chlorophyll is out of the plotting range (minimum value of that curve is 0.2, with a shape similar to the black curve).

6. CORRECTION OF STRAYLIGHT

Straylight errors may be corrected mathematically if an instrument is fully characterized for all PSFs. However, algorithms used previously are generally based on deconvolution approaches that consume a large amount of computing time and are mainly effective with (and focused on) restoring high frequency components of blurred images.^{6,12-14}

A new practical method, tailored for correction of straylight errors, was developed recently.^{15,16} Instead of sharpening an image, the new method is developed for correcting the small amount of out-of-field of the resolving power straylight within the instruments FOV, and the correction is simply a matrix multiplication of a constant correction matrix to any measured raw image. We plan to apply straylight corrections to MODIS images using the derived the PSFs (discussed above) and the new straylight correction method. The new method is summarized below. Suppose we have derived a set of PSFs (for a subset of pixels of an instrument) covering an instrument's field-of-view, each PSF can be used to derive a straylight distribution function (SDF): the ratio of the straylight signal to the total signal within the field of resolving power of the instrument. By using the set of derived SDFs and perform interpolation between these SDFs and extrapolation beyond these SDFs, the SDF for every pixel can be obtained. Each of the 2-dimensional SDFs is then transformed to a 1-dimensional column vector. By using all of the column vector SDFs, a SDF matrix, denoted \mathbf{D} , can be constructed. The SDF matrix \mathbf{D} is then used to derive the straylight correction matrix \mathbf{C}_{spat} . The straylight errors in the raw image can be corrected by using Equation 3,

$$\mathbf{Y}_{\text{IF}} = \mathbf{C}_{\text{spat}} \mathbf{Y}_{\text{meas}}, \quad (3)$$

where \mathbf{C}_{spat} is a constant matrix (and thus the development of \mathbf{C}_{spat} is required only once unless the imaging characteristics of the instrument change), \mathbf{Y}_{meas} is the column vector of the measured raw image signals obtained by transforming 2-dimensional imaging signals, and \mathbf{Y}_{IF} is the column vector of the straylight corrected image signals. Using Equation 3, the straylight correction becomes a single matrix multiplication. Note that the derived PSFs also include other types of errors from the instrument (e. g. smearing in the scan direction, and the detector window reflection, etc.), thus, a straylight correction eliminates other types of errors as well.

The new method has been used for correcting straylight errors in a high-quality commercial 12-bit, 1.4 million pixel CCD-array imaging radiometer. The straylight-corrected imaging radiometer was used to measure radiance of an integrating sphere source at the circular exit port where a black baffle was hung at the center. The size of the exit port was adjusted to be smaller than the field-of-view of the imaging radiometer, so that the straylight signals arising from the source outside the field-of-view of the imaging radiometer were theoretically zero. Shown in Figure 11 is the result of correction for the measurement of the integrating sphere source, which is a plot of 1-dimensional signals along a center line across the sphere exit port. The maximum signal (not plotted) is normalized to one. It is clear that the level of straylight in the black baffle region reaches 10^{-2} (even with this high-quality imaging radiometer), which is significant, and it is reduced by more than one order of magnitude after the straylight correction is applied.

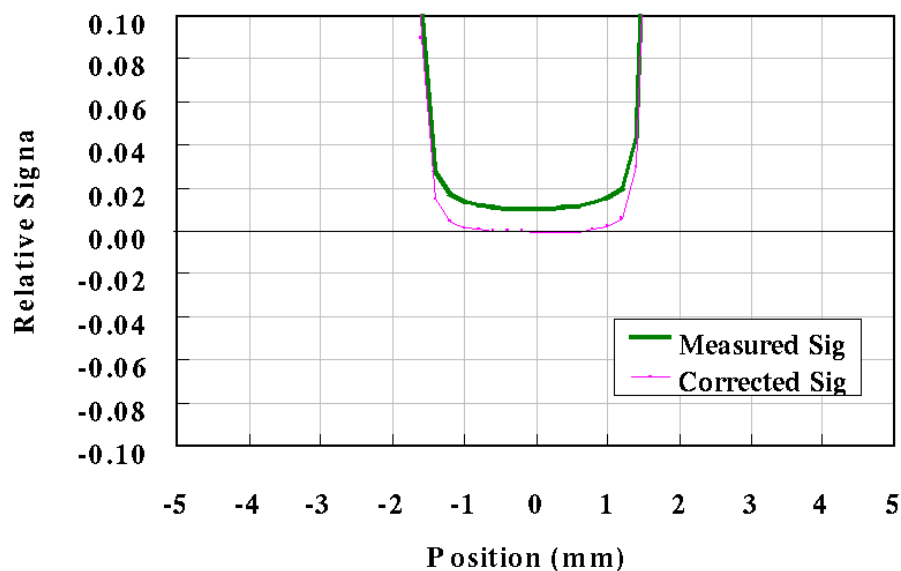


Figure 11. Results of stray-light correction for a CCD-array imaging radiometer.

7. CONCLUSIONS

The PSF presented here is preliminary and requires further testing. We are planning to apply the correction outlined in section 6 to real MODIS data to quantify the effect of straylight on the retrieval of chlorophyll, water-leaving radiance, and AOT (aerosol optical thickness). Currently, a 5x7 mask (5 pixels in track direction, 7 pixels in scan direction) is applied around cloud pixels, which has significantly improved the agreement between the AOT of MODIS Aqua and the SeaWiFS sensor, see Franz et al.⁹ This mask indeed removes the steepest part of the L_t curves, see Fig. 9.

The effects of the MODIS PSF as presented here are substantial. We are not sure yet whether they are real, or largely due to an inaccurate characterization. Either way, this underscores the need for a high quality prelaunch straylight characterization for remote sensing ocean color sensors.

Fig. 10 suggests that without a straylight correction, the water-leaving radiances of MODIS Aqua depend on the distance to the nearest cloud. This result is preliminary, but if confirmed, we expect the straylight correction algorithm to reduce this dependency.

ACKNOWLEDGMENTS

We want to thank Roger Drake from SBRS/Raytheon, who provided the MODIS Aqua prelaunch characterization data (NFR measurements).

REFERENCES

- [1] Barnes, W. L., Pagano, T. S., and Salomonson, V. V., "Prelaunch characteristics of the Moderate Resolution Imaging Spectroradiometer (MODIS) on EOS-AM1," *IEEE Transactions on Geoscience and Remote Sensing* **36**, 1088–1100 (1998).
- [2] Hurt, T. and Derrick, P., "MODIS FM1 Near Field Response," *Raytheon, Interdepartmental Correspondence Ref PL3095-N07729 Rev A* (2000).
- [3] Derrick, P., "MODIS FM1 Harvey-Shack scattering model analysis," *Raytheon, Interdepartmental Correspondence Ref PL3095-N07881* (2002).
- [4] Young, J. B., "Point Spread Function (PSR) near field response measurement methodology - revision," *SBRS internal memorandum Ref PL3095-N05401* (1995).
- [5] Nishihama, M., [*MODIS Level 1A Earth Location: Algorithm Theoretical Basis Document Version 3.0*], NASA, Goddard Space Flight Center (1997).
- [6] Qiu, S., Godden, G., Wang, X., and Guenther, B., "Satellite-Earth remote sensor scatter effects on Earth scene radiometric accuracy," *Metrologia* **37**, 411–414 (2000).
- [7] Koren, I., Remer, L. A., Kaufman, Y. J., Rudich, Y., and Martins, J. V., "On the twilight zone between clouds and aerosols," *Geophys. Res. Lett.* **34**(L08805) (2007).
- [8] Redemann, J., Zhang, Q., Russel, P. B., Livingston, J. M., and Remer, L. A., "Case studies of aerosol remote sensing in the vicinity of clouds," *Geophysical Research Letters* **submitted** (2008).
- [9] Franz, B. A. and 9 co-authors, "The continuity of ocean color measurements from SeaWiFS to MODIS," **5882**, 58820W, SPIE (2005).
- [10] Yeh, E., Barnes, R., Darzi, M., Kumar, L., Early, E., Johnson, B., Mueller, J., and Trees, C., [*Case Studies for SeaWiFS Calibration and Validation, Part 4*], vol. 41 of *NASA Technical Memorandum 104566, SeaWiFS Technical Report Series*, NASA, Goddard Space Flight Center (1997).
- [11] Gordon, H. and Wang, M., "Retrieval of water-leaving radiance and aerosol optical thickness over the oceans with seawifs: a preliminary algorithm," *Applied Optics* **33**(3), 443–452 (1994).
- [12] Jeffries, S. M. and Christou, J. C., "Restoration of astronomical images by iterative blind deconvolution," *The Astrophysical Journal* **415**, 862–874 (1993).
- [13] Keel, W., "A simple, photometrically accurate algorithm for deconvolution of optical images," *Publications of the Astronomical Society of the Pacific* **103**, 723–729 (1991).
- [14] Li, H., Robinson, M. S., and Murchie, S., "Preliminary remediation of scattered light in NEAR MSI images," *Icarus* **155**, 244–252 (2002).
- [15] Zong, Y., Brown, S. W., Johnson, B. C., Lykke, K. R., and Ohno, Y., "Correction of stray light in spectroradiometers and imaging instruments," **CIE 178**, D2–33–D2–36, CIE (2007).
- [16] Zong, Y., Brown, S. W., Meister, G., Barnes, R. A., and Lykke, K. R., "Characterization and correction of stray light in optical instruments," **6744**, 67441L–1–11, SPIE (2007).